AIAA 94-0314

Skin-Friction Measurements in a 3-D, Supersonic Shock-Wave/Boundary-Layer Interaction

J.K. Wideman
University of Missouri
Columbia, MO

J.L. Brown
NASA Ames Research Center
Moffett Field, CA

J.B. Miles
University of Missouri
Columbia, MO

O. Ozcan
Istanbul Technical University
Istanbul, Turkey

32nd Aerospace Sciences Meeting & Exhibit
January 10-13, 1994 / Reno, NV

RFE:229-1/005

Dr. George W. Sutton
Editor-in-Chief AIAA Journal
P.O. Box 15627
Arlington, VA 22215-0627

Dear Dr. Sutton:

Enclosed are five copies of the manuscript entitled Skin-Friction Measurements in a 3-D, Supersonic Shock-Wave/Boundary-Layer Interaction, by J. K. Widman, J. L. Brown, J. B. Miles, O. Ozcan, which Ames Research Center wishes to submit to the AIAA Journal. This manuscript is not classified and has not been submitted elsewhere. Attached is a list of five suggested reviewers.

Sincerely,

James L. Brown
Research Scientist
Modeling and Experimental Validation Branch

VLP
FRB
PK
JGM
JLBrown:jlj 11/04/93 - 45397

SKIN-FRICTION MEASUREMENTS IN A 3-D, SUPERSONIC SHOCK-WAVE/BOUNDARY-LAYER INTERACTION

Jeffrey K. Wideman*
University of Missouri
Columbia, Missouri

James L. Brown**
NASA Ames Research Center
Moffett Field, California

John B. Miles†
University of Missouri
Columbia, Missouri

Oktay Ozcan‡
Istanbul Technical University
Istanbul, Turkey

Abstract

The experimental documentation of a three-dimensional shock-wave/boundary-layer interaction in a nominal Mach 3 flow is presented. The model consisted of a sting-supported cylinder, aligned with the free-stream flow, and a 20° half-angle conical flare offset 1.27 cm from the cylinder centerline. Surface oil flow, laser light sheet illumination, and schlieren were used to document the flow topology. The data includes surface-pressure and skin-friction measurements. A laser interferometric skin friction instrument was employed to acquire the skin-friction data. Included in the skin-friction data are measurements within separated regions and three-dimensional measurements in highly-swept regions. The skin-friction data will be particularly valuable in turbulence modeling and computational fluid dynamics validation.

Nomenclature

C_f	local skin-friction coefficient ($\equiv \tau / \frac{1}{2}\rho_\infty U_\infty^2$)
$C_{1,2,3}$	constants
h	local oil thickness
k_i	incremental fringe number
M_∞	free-stream Mach number
n_o	refractive index of oil
N	fringe number
N_o	reference fringe number
P	local surface pressure
P_t	total pressure
P_∞	free-stream static pressure
r	radial coordinate from cylinder centerline
Re	Reynolds number
t	oil-flow time
t_i	incremental oil-flow time
t_o	reference oil-flow time
T_t	total temperature
T_∞	free-stream static temperature
U_∞	free-stream velocity
x	streamwise coordinate, also distance from oil leading edge to measurement beam
x_a	attachment location
x_s	separation location
z	transverse coordinate
β	surface flow angle
δ	boundary-layer thickness
θ_t	refracted beam angle
κ	Von Kármán constant
λ	wavelength of light
ν_o	kinematic viscosity of oil
ρ_o	density of oil
ρ_∞	free-stream density
ϕ	azimuthal coordinate
τ	local shear stress at the wall

Introduction

The flow field surrounding aerodynamic vehicles can be quite complex. The nature of practical flows are typically compressible, turbulent, and three-dimensional (3-D). In addition, at supersonic speeds shock waves exist which interact with the boundary layers on flight surfaces. The adverse pressure gradient associated with shock-wave/boundary-layer interactions (SW/BLI) can cause the boundary layer to separate, thus altering aircraft performance. Hence, there is a need to better understand and predict these SW/BLI.

Over the years, computational fluid dynamics (CFD) has augmented the experimental research on SW/BLI. Although the idea of a full computational simulation of flow fields instead of wind tunnel documentation is appealing, much work needs to be done before complete computational solutions to 3-D SW/BLI problems can be reliably achieved. In solving the Navier–Stokes equations, closure of the equation set is achieved by modeling the turbulence. These turbulence models need to be developed through reliance on measurements of the physical phenomenon of the interaction. There is also a need to provide experimental data to validate the computational results from CFD. Thus, experiments and computations are complementary tools that can extend the present understanding of fluid dynamics and produce methods by which SW/BLI can be accurately predicted.

*Ph.D. Student, Student Member AIAA

**Research Scientist

†Professor of Mechanical Engineering, Member AIAA

‡Professor

AIAA 32nd Aerospace Sciences Meeting and Exhibit, January 10-13, 1994, Reno, NV.

The present study was undertaken with the goal of acquiring accurate data in a 3-D SW/BLI in order to guide the development of turbulence modeling and the validation of CFD codes. Because of the scarcity of accurate skin-friction data in SW/BLI, the emphasis of this study was on the acquisition of skin-friction data. A laser interferometric skin friction (LISF) instrument was used to acquire the skin-friction data in a complex flow characterized by large pressure and shear gradients where the reliability of other techniques would be questionable.

Experimental Description

Flow Model and Test Conditions

The experimental study was conducted at NASA Ames Research Center in the High Reynolds Number Channel I (HRC-I) wind tunnel. A Mach 3 nozzle was employed for the study. The test section was 25.4 cm wide by 38.1 cm high. The axisymmetric boundary layer developed on a 5.08 cm diameter stainless steel cylinder aligned with the tunnel axis (Figs. 1 and 2). The instrumented 3-D flare slid over and was secured to the downstream cylindrical section. The flare was fabricated as if it were a 20° half-angle axisymmetric cone with its centerline displaced 1.27 cm from the centerline of the cylinder axis. The flare was terminated with a 12.70-cm-diameter afterbody, the centerline of which matched that of the cylinder. The two azimuths of symmetry were along $\phi = 0°$ and $\phi = 180°$. The x–ϕ–r coordinate system was a cylindrical system aligned with respect to the cylinder centerline axis with $x = 0$ cm located at the leading edge of the offset flare. The model was chosen because the resulting shock system was found to be steady via spark schlieren. The average tunnel operating conditions are summarized in Table 1.

Pressure Measurement

Surface pressures were measured through pressure taps on the cylinder and on the 20° 3-D flare by an electronic scanning pressure system from Pressure Systems, Inc. The strain gage differential transducers were referenced to the upstream static pressure, which was sensed by a 1000 torr absolute Barocell. Each transducer was calibrated prior to every run. The total pressure was sensed by a 100 psi differential Barocell referenced to atmospheric conditions. The instrumented cylinder possessed four rows of pressure taps along azimuths spaced 90° apart. The flare contained 13 rows of 22 pressure taps that could document one region of symmetry ($\phi = 0°$–$180°$) in intervals of 15°.

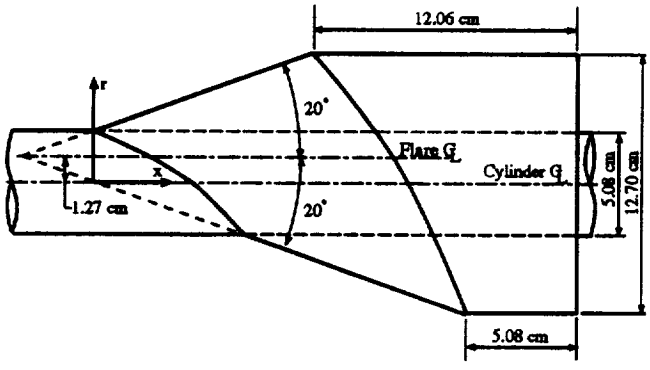

Fig. 1 Schematic of 20°/1.27 cm offset 3-D flare.

Table 1. Average tunnel operating conditions

P_t	172.37 kPa (1.7 atm)
T_t	280 K
P_∞	5.54 kPa
T_∞	105 K
ρ_∞	0.184 kg/m^3
M_∞	2.89
U_∞	593 m/s
Re	15.0×10^6 1/m
δ	1.10 cm

Skin Friction Measurement

Theory–Since Tanner and Blows[1] first introduced the theoretical basis for the LISF technique there have been many different approaches to implementing the theory. In addition to the work done by Tanner and his associates, other significant studies involving the LISF technique have been performed at NASA Ames Research Center,[2,3] Pennsylvania State University,[4] and at the California Institute of Technology.[5] The LISF technique is nonintrusive and is quasi-direct in determining the shear stress at the wall. The technique does not require calibration. Since its inception, the complexity of the flows to which the LISF technique has been applied has increased. It is in these complex flows, such as SW/BLI, that the real advantage of the LISF technique comes to light because it is capable of performing accurate skin-friction measurements in flows characterized by large pressure and shear gradients. A more thorough review of the LISF technique and additional technical information can be found in Ref. 6.

Briefly, the LISF technique requires a thin film of oil on the test surface. The thickness of the oil film decreases with time due to the wall shear stress of the air flow. To measure the time-dependent thickness of this oil film, a focused laser beam is directed toward the oil. A portion of the laser beam is reflected from the air–oil interface and another portion is reflected from the oil–model interface. The light reflected from the two interfaces is imaged onto a photocell using collecting lenses. The path length of the light reflected from these two interfaces from the laser to the photocell differs according to the oil–film thickness. As the oil film thins, a time sequence of interference fringes occurs at the photocell due to this varying path length difference. The time-varying voltage output of the photocell is referred to as the fringe record and consists of a series of peak and valleys related to the time-varying oil thickness.

An oil film subjected to a constant shear stress will assume a wedge shape. For this case, the basic LISF equation[1]

for the shear stress is

$$\tau = \frac{\rho_o \nu_o x}{ht} \tag{1}$$

where τ is the local shear stress at the wall, ρ_o is the oil density, ν_o is the oil kinematic viscosity, x is the distance between the measurement beam and the oil leading edge, h is the local oil thickness, and t is the oil-flow time. This equation is valid for flows free of pressure-gradient effects, shear-gradient effects, and gravity effects. Under these conditions the equation determining the shear stress at the wall is independent of the properties of the boundary layer.

From refraction theory, the thickness of the oil film can be determined from the equation

$$h = \frac{N\lambda}{2n_o \cos\theta_t} \tag{2}$$

where N is the fringe number, λ is the wavelength of the laser beam, n_o is the refractive index of the oil, and θ_t is the angle of the refracted laser beam. Combining Eqs. (1) and (2), the expression for the wall shear stress becomes

$$\tau = \frac{2n_o \rho_o \nu_o x \cos\theta_t}{N\lambda t} \tag{3}$$

Under swept conditions, the component of skin-friction in a particular direction can be measured by initially applying the oil perpendicular to the measurement axis.

Apparatus–A schematic of the LISF instrument is shown in Fig. 2. The transmitting side of the instrument included a 5.0 mW helium–neon laser that produced a coherent light beam at a wavelength of 0.6328 μm. A spatial filter and a combination of lenses expanded the beam and allowed adjustment of the beam focus location. A 6.330-mm-thick interferometric flat made of fused silica was used to split the beam. By positioning the flat at a 45° angle with respect to the incident beam; the reflection from the front and the back of the flat provided two beams of nearly the same intensity with a spacing of 5 mm. A vertical assembly containing several mirrors directed the two laser beams into the tunnel and toward the model at a near-normal incidence angle. Even though two beams were available, the single-beam approach was used to perform the LISF measurements partly because of the relatively small scale of the interaction under study.

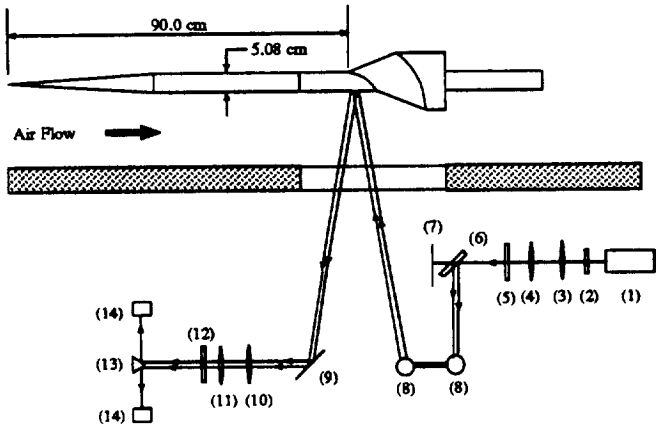

(1) 5.0 mW helium-neon laser
(2) Spatial filter
(3) Focusing lens
(4) Focusing lens
(5) Neutral density filter
(6) Interferometric flat
(7) Beam stop
(8) Vertical assembly of mirrors
(9) Mirror
(10) Collimating lens
(11) Focusing lens
(12) 0.6328 micron filter
(13) Reflective prism
(14) Photodiodes

Fig. 2 Schematic of HRC-I LISF instrument.

The receiving side of the instrument included lenses to collimate and focus the reflected light from the two measurement spots onto different sides of a reflective-coated prism. The prism directed the beams into two separate photodiodes. The signals were amplified, low-pass filtered, and then digitized. The laser and the optics were located on an optical table which was controlled in the vertical and streamwise directions by two stepper motors. The oils used were Dow Corning "200" Silicon Fluids with three different nominal viscosities: 200, 500, and 1000 cs.

The properties of the model surface upon which LISF measurements are performed are important. First, the surface should be smooth and free of imperfections (such as scratches). Second, the intensity of the reflected beam from the oil-model interface should be comparable to the intensity of the reflected beam from the air–oil interface to maximize signal visibility. An alternative to the often used technique of polishing the test surface was sought. First, a layer of Monokote was applied to the surface. Then a clear plastic[7] with an adhesive backing was placed over the Monokote. The clear plastic provided a smooth surface where the oil could flow and also reflected a portion of the incident beam that was comparable to the intensity of the reflection from the air–oil interface contributing to a signal visibility of typically 60% (Fig. 3). The zero level of the ordinate in the plot is the actual zero voltage level. The Monokote covered the model surface and absorbed the portion of the incident beam

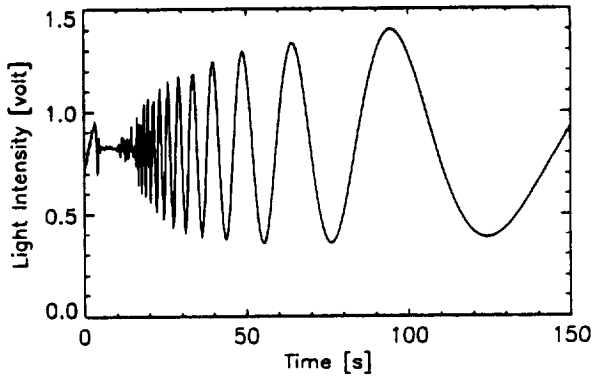

Fig. 3 LISF signal from plastic surface over Monokote.

that passed through both the oil and the clear plastic. The Monokote and clear plastic guarded against any interference from the pressure taps on the LISF measurements. A second similar technique of preparing the model surface was to spray paint the surface black and then attach the clear plastic.

Since the oil viscosity was sensitive to temperature, an accurate measure of the surface temperature was crucial for the accurate determination of skin friction with the LISF technique. The oil thickness was extremely thin so the temperature of the oil was assumed to equal the surface temperature. The flare was fabricated with an internal iron–constantan thermocouple located at $x = 12.5$ cm along $\phi = 90°$. An extensive effort was put forth to verify the accuracy of the temperature reading from this thermocouple. One consideration was the possible effect of the clear plastic between the model surface and the oil. The effect, however, was negligible because the temperature difference across the plastic was estimated to be only 0.6 K. With only one thermocouple available, the temperature of the entire model was assumed to equal the reading from this thermocouple. In light of this assumption and the inherent difficulty in measuring the surface temperature, the oil viscosity term was the source of the largest uncertainty in the final skin-friction result.

Data Reduction–The pertinent quantity to be determined from the LISF fringe record is the product of the fringe number and time (Nt). The following analysis was suggested by Stan Bouslog[8] in order to accurately determine a value for the fringe-time product from LISF data. Equation (3) can be rearranged to obtain

$$\frac{1}{N} = \frac{\tau\lambda}{2n_o\rho_o\nu_o x\cos\theta_t}t = C_1 t \tag{4}$$

where C_1 may be assumed constant due to steady shear stress and oil temperature as given by

$$C_1 \equiv \frac{\tau\lambda}{2n_o\rho_o\nu_o x cos\theta_t} \tag{5}$$

A reference fringe extreme (peak or valley) can be arbitrarily selected from the experimentally obtained fringe record. A reference fringe number (N_o) and time (t_o) can be assigned to an extreme even though the actual values are unknown. Inserting these reference variables into the previous equation yields

$$\frac{1}{N_o} = C_1 t_o \tag{6}$$

Proceeding through the rest of the fringe record, each successive extreme is assigned an incremental fringe number (k_i) that is incremented by one-half for each extreme. Thus, some extreme occurring in time after the reference fringe may be identified by its fringe number and time as given by

$$N = N_o - k_i\ ,\ t = t_o + t_i \tag{7}$$

where t_i represents the incremental time. These two expressions can be inserted into Eq. (4) to obtain

$$\frac{1}{N_o - k_i} = C_1(t_o + t_i) = C_1 t_o + C_1 t_i \tag{8}$$

Recalling that $C_1 = 1/N_o t_o$ and introducing two new constants, the previous equation can be rearranged to read

$$k_i = \frac{t_i}{C_2 + C_3 t_i} \tag{9}$$

where the constants are defined as

$$C_2 \equiv \frac{t_o}{N_o}\ ,\ C_3 \equiv \frac{1}{N_o} \tag{10}$$

The incremental values for the fringe number and time, k_i and t_i, in Eq. (9) are obtained from the LISF fringe record once a reference fringe is chosen and plotted (Fig. 4). The data point for the reference fringe was located at the origin of the plot. The time at which the flow began does not need to be known for this analysis. The two unknown constants C_2 and C_3 are determined by performing a least-squares curve fit of Eq. (9) to the incremental fringe number versus time data as shown in Fig. 4. The two constants can be combined to determine the constant C_1 from the equation

$$C_1 = \frac{C_3^2}{C_2} \tag{11}$$

By rearranging Eq. (5), the local shear stress at the wall can be calculated from

$$\tau = \frac{2n_o\rho_o\nu_o x cos\theta_t\ C_1}{\lambda} \tag{12}$$

Finally, the shear stress can be nondimensionalized by upstream free-stream conditions using

$$C_f \equiv \frac{\tau}{\frac{1}{2}\rho_\infty U_\infty^2} \tag{13}$$

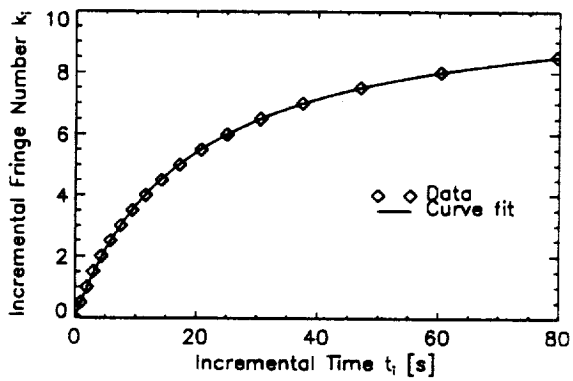

Fig. 4 Curve fit of incremental fringe number vs. time.

where C_f is the local skin-friction coefficient.

In the preceding derivation, the surface temperature was assumed steady. This assumption was not valid for this supersonic test. The temporal variation of the surface temperature, and hence the oil temperature, was accounted for by using a corrected time based on the temperature variation.[6] Also, nonzero pressure or shear gradients can affect the shape of the oil film and thus affect the LISF measurements. Using the analysis of Monson, Driver, and Szodruch,[2] the correction required for each LISF measurement was determined. The corrections, however, were not significant. Thus, the skin-friction results presented in this paper were not corrected for these effects.

Results and Discussion

Surface Flow Visualization

Surface oil-flow visualization revealed many details of the surface topology. Figures 5 and 6 are two views of the model after one run. Figure 7 shows an oil-streak pattern after a different run and provides more detail in the region

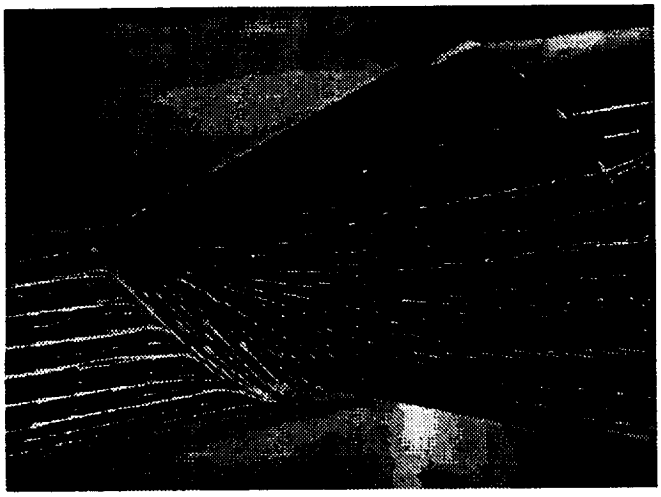

Fig. 5 Oil-flow visualization (view from $\phi \approx 45°$).

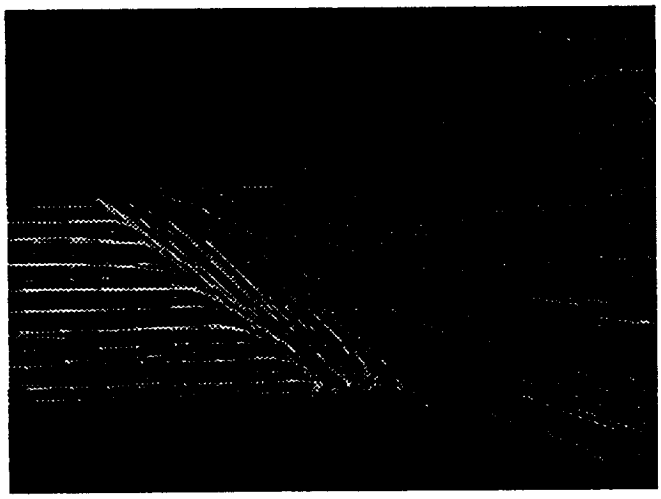

Fig. 6 Oil-flow visualization (view from $\phi \approx 90°$).

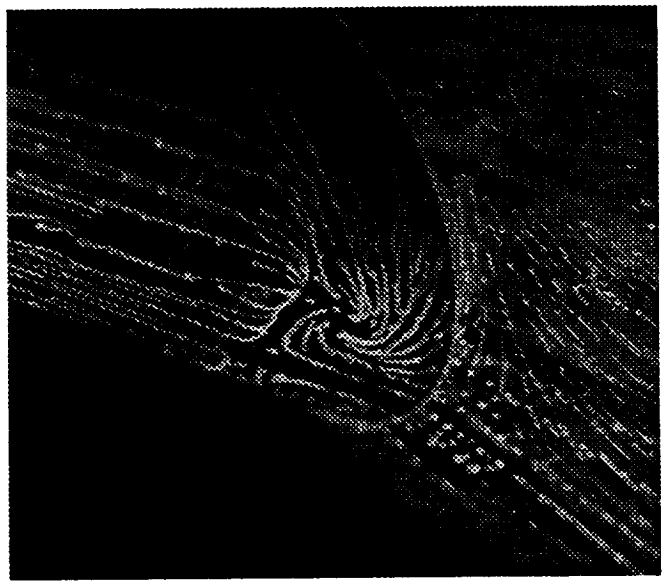

Fig. 7 Oil-flow visualization (view from $\phi \approx 165°$).

near the $\phi = 180°$ line of symmetry. The flow in these figures was from left to right. The postulated skin-friction pattern is shown in Fig. 8. There were a total of seven nodes and five saddles which satisfied the topological law[9] (for a closed 3-D surface, the number of nodes must exceed the total number of saddles by two (7 nodes−5 saddles = 2)). Although not shown, there was a front nodal point of attachment ($N6$) located on the upstream tip of the cylinder and a nodal point of separation ($N7$) located at the rear of the cylinder.

Referring to Figs. 5–8, a saddle of separation ($S1$) and a node of attachment ($N1$) were formed along $\phi = 0°$. The separation lines that emanated from the saddles of separation along $\phi = 0°$ ($S1$) and $\phi = 180°$ ($S4$) terminated

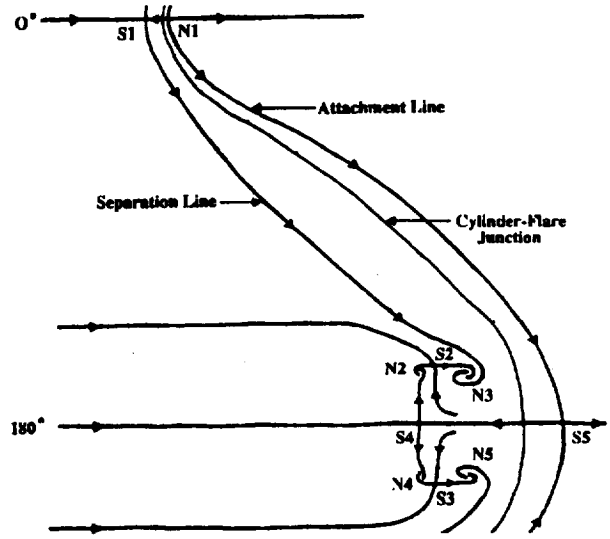

Fig. 8 Unwrapped postulated skin-friction pattern.

into different foci of separation ($N3$ and $N2$). Another saddle of separation ($S2$) was interspersed between these two foci. A saddle of attachment ($S5$) was formed at the intersection of the attachment line and $\phi = 180°$ and was directly connected to saddle of separation $S4$. This type of connection was traditionally thought to be unstable. It is possible that the resolution of the oil flows was not adequate to distinguish other singular points in the vicinity of saddle S5. Yet Chapman[10] considered saddle-to-saddle connections possible under conditions of strong symmetry. Other references[11,12] also featured such connections. Thus, the present saddle-to-saddle connection along $\phi = 180°$ is plausible as a consequence of the flow symmetry.

Based on the surface oil flows, schlieren, and laser light sheet visualization techniques, a postulated flow structure was developed. The spark schlieren visualization indicated that the shock system was steady. The flow structure along $\phi = 0°$ consisted of separation, which spiraled into a vortex, followed by attachment on the flare. The vortex continued along the model on both sides of symmetry. Near $\phi = 180°$, the postulated flow structure included two main vortices which left the surface at the two largest foci of separation ($N3$ and $N5$) and remained embedded within the boundary layer on the flare.

Surface Pressure

The data presented here consists of pressure measurements with the model rotated so the desired azimuths were aligned with the top of the cylinder. The accuracy of the measurements was estimated to be within 1% of P/P_t. The pressure distributions along individual azimuths are shown in Fig. 9. A contour plot of the pressure data is shown in Fig. 10. The contours reveal the steep streamwise pressure gradient along $\phi = 0°$. There is also a steep streamwise pressure gradient in the region between $\phi = 150°$ and $\phi = 180°$ on the cylinder. The transverse pressure gradient is apparent in the plot between $\phi = 15°$ and $\phi = 150°$. The direction of the maximum pressure gradient appeared to be roughly normal to the cylinder–flare junction. The plateau regions visible in the individual distributions are evident in the contour plot downstream of the initial pressure rise and upstream of the cylinder–flare junction from $\phi = 30°$ to $\phi = 180°$. The wavy contour line in the region near the cylinder–flare junction is due to the disparity of the amount of data taken in the transverse direction as compared to the streamwise direction and is an artifact of the contour calculation. The contour plot is overlaid with the interpretation from the oil-flow visualization results. The scale of Fig. 10 was chosen to allow the overlay of Fig. 8.

Skin Friction

Measurements in Undisturbed Boundary Layer–In contrast to the pressure measurements (for reasons of optical access), the skin-friction data was acquired with the model rotated so the desired azimuths were aligned with the side of the cylinder. To assess the accuracy of the LISF measurements in the undisturbed boundary layer upstream of the

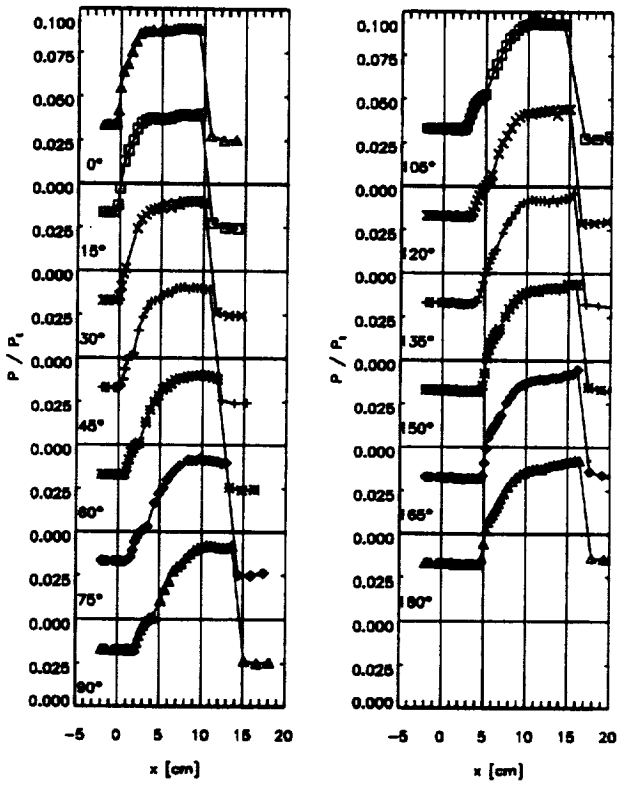

Fig. 9 Surface pressure distributions.

interaction, a comparison was made to results from other techniques. There are instruments that accurately measure the skin friction in boundary layers free of pressure- and shear-gradient effects. However, such instruments were not available for this study. Thus, other standards for comparison were pursued. One of these standards employed a similarity technique to deduce the skin friction from the experimental mean-velocity profiles. The velocity profiles were acquired with a 3-D laser Doppler velocimetry (LDV) system. The analysis of Sun and Childs[13] was applied to the experimental velocity profiles by curve fitting their wall–wake correlation to the data. The mean of the deduced skin-friction results was $C_{f_x} = 0.00144\ (\pm 2\%)$. A second standard was the Van Driest (II) theory[14] derived for a flat-plate flow. The theory predicted a skin-friction coefficient of $C_{f_x} = 0.00156$. The mean skin-friction coefficient from the LISF measurements was $C_{f_x} = 0.00149\ (\pm 5\%)$ which was 3% higher than the deduced value from the velocity profile and 5% lower than the value predicted by the Van Driest (II) theory. Since the value of the LISF result was between the two selected standards, it provided sufficient confidence that the LISF result in the undisturbed boundary layer was accurate.

Measurements along $\phi = 0°$–As the boundary layer initially encountered the streamwise pressure gradient, the mean flow near the wall was retarded decreasing the skin friction (Fig. 11). A linear extrapolation of the skin-friction

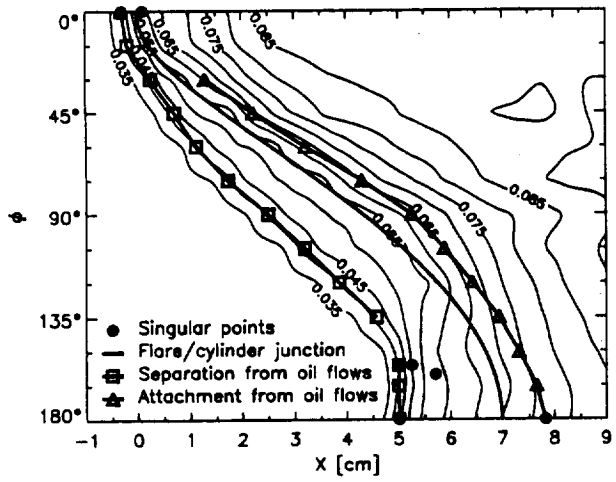

Fig. 10 Surface-pressure contour plot based on P/P_t.

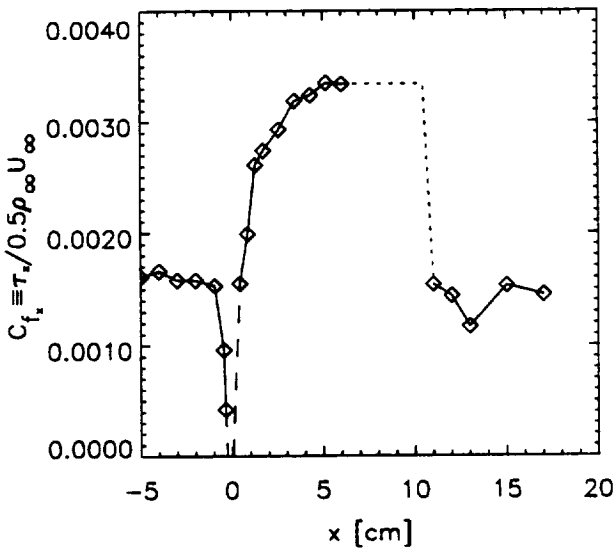

Fig. 11 Streamwise LISF measurements along $\phi = 0°$.

data upstream of separation down to the zero skin-friction level indicated that separation occurred at $x_s = -0.27$ cm. This extrapolated location was comparable to the separation location from the surface oil-flow visualization technique which was estimated to be at $x_s = -0.30$ cm. Continuing along this line of symmetry, it is expected that the sign of the skin friction would be negative in the separated region since the oil-flow visualizations revealed that the flow direction was opposite to the free-stream direction. However, the distance between the separation line and cylinder–flare junction along $\phi = 0°$ was too small to perform a measurement. Dashed lines in Fig. 11 indicate the expected distribution just upstream of separation and downstream of attachment.

At the first measurement location downstream of attachment, the skin friction had increased significantly from the anticipated negative values in the separated region to a level comparable to the undisturbed value. In contrast to a closed two-dimensional separation bubble, 3-D separation can entrain fluid. As the flow proceeded over the separated region along this azimuth, the innermost low-momentum fluid of the boundary layer was entrained into the 3-D separation vortex. Thus, the flow that attached consisted of only the outer, more energetic fluid of the original boundary layer which immediately imposed a steep velocity gradient at the surface. Further, as a result of the interaction, the increased turbulent activity led to increased mixing. This accelerated the lower portion of the redeveloping boundary layer and increased the velocity gradient which contributed to an increased skin friction.

The pressure reached a peak plateau at $x = 2.35$ cm. The skin friction continued to increase beyond that point and eventually reached a plateau near $x = 5.17$ cm. The overall pressure-rise ratio along $\phi = 0°$ was equal to 2.59. The overall rise in the skin-friction coefficient along this same azimuth was 2.25 (a 125% increase). Thus, one effect of the interaction was a doubling of the local skin friction along this azimuth. The pressure measurements for this model rotation (not shown) indicated the presence of an extraneous shock wave from the tunnel wall near the aft end of the flare ramp. As a consequence, the skin-friction measurements in this vicinity jumped in value and are not shown.

Measurements along $\phi = 90°$–The flow along $\phi = 90°$ was not only affected by the streamwise pressure gradient, but also by the transverse pressure gradient. After an initial drop, the streamwise skin friction leveled out just prior to separation and maintained a slightly decreasing trend to a location just inside the 3-D separation (Fig. 12). For 3-D separation, the skin friction is equal to zero only along the direction normal to the separation line and separation does not imply that the streamwise skin friction should be negative. This is true for the streamwise data along $\phi = 90°$ where the skin friction did not become negative in the separated region. The oil-flow visualizations indicated that the separation line was at $x_s = 2.50$ cm at which point the streamwise skin friction was estimated to be $C_{f_x} = 0.00080$.

Toward the middle of the separated region along $\phi = 90°$, the skin friction distribution reached a minimum at $x = 3.85$ cm. Between $x = 3.75$ cm and $x = 4.00$ cm, the pressure in the streamwise direction was nearly constant, increasing by only 0.4%. One measurement location on the flare within the separated region indicated a sharp increase in skin friction. The streamwise skin friction was higher in the vicinity of attachment than it was near separation. Attachment was located on the flare at $x_a = 5.25$ cm as indicated by oil-flow visualizations. The streamwise skin friction began to level off near $x = 10.0$ cm, which was slightly downstream from the plateau in the pressure distribution. The

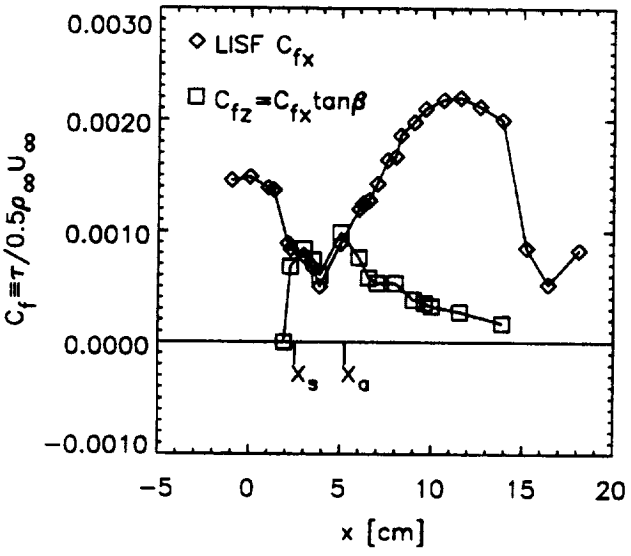

Fig. 12 Streamwise LISF measurements along $\phi = 90°$.

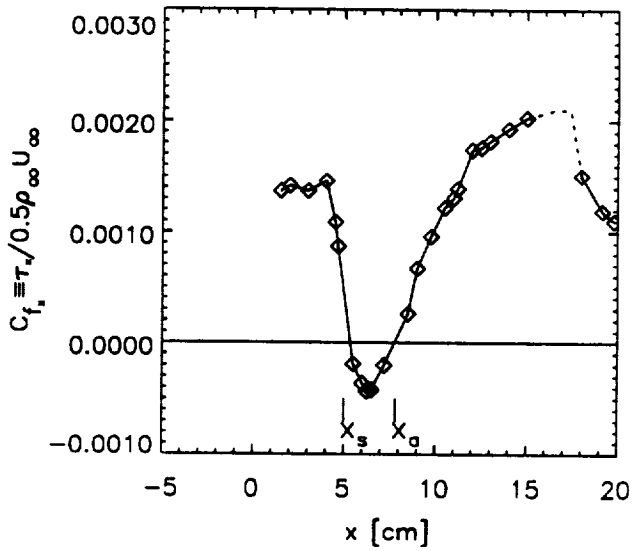

Fig. 13 Streamwise LISF measurements along $\phi = 180°$.

peak value for the streamwise skin-friction coefficient along $\phi = 90°$ was $C_{f_x} = 0.00220$ and was an increase of 48% over the undisturbed level.

The values for the component of skin friction in the transverse direction (Fig. 12) were resolved from the streamwise LISF measurements and the flow-angle data from oil-flow visualization. As a result of the transverse pressure gradient, the flow in the upstream influence region along $\phi = 90°$ immediately began turning away from the free-stream direction. The skin-friction coefficient in the transverse direction increased from zero in the undisturbed boundary layer to a value of $C_{f_z} = 0.00068$ at $x = 2.25$ cm. The transverse skin-friction coefficient reached a relative maximum at $x = 3.00$ cm, 0.50 cm downstream of separation. The transverse skin friction reached another maximum just upstream of attachment. Downstream of attachment, the transverse distribution demonstrated the turning of the flow toward the conical direction. LISF measurements in the transverse direction were performed at six different locations upstream and within the separated region. These particular measurements agreed with the resolved values to within 5%. The maximum flow-turning angle with respect to the free-stream direction was determined from the oil–flow visualization to be 50° at $x = 3.85$ cm.

Measurements along $\phi = 180°$–The initial effect of the interaction along $\phi = 180°$ was evidenced by a drop in the streamwise skin friction just upstream of $x = 4.5$ cm. Within the separated region, the flow direction along $\phi = 180°$ was opposite to the free-stream direction. Skin-friction measurements were performed at five locations within the separated region as indicated by the negative values of skin friction in Fig. 13. Four of these measurement locations were on the cylinder and one was on the flare. Within the separated region, the largest absolute magnitude measurement was $|C_{f_x}| = 0.00043$, which was 29% of the undisturbed value. These measurements within the separated region are of particular importance since accurate skin-friction data in separated flows is scarce.

Interpolation between the skin-friction measurements upstream and downstream of separation gave the location of separation at $x_s = 5.20$ cm. The pressure measurements indicated that separation was at $x_s = 5.25$ cm while the oil-flow visualization indicated separation was at $x_s = 5.00$ cm. Interpolation of the skin-friction data near attachment indicated its location to be at $x_a = 7.8$ cm which coincided with the attachment location as determined from oil-flow visualization. The pressure distribution reached a peak plateau at $x = 9.25$ cm. The maximum skin-friction coefficient of $C_{f_x} = 0.00203$ was reached at the most downstream measurement location on the ramp, but the skin-friction distribution appeared to have still been increasing. This value was 41% larger than the undisturbed level. The peak level along $\phi = 180°$ was much lower than the peak level along $\phi = 0°$ partially as a consequence of the thicker boundary layer that existed along $\phi = 180°$. Additional features, such as the presence of the vortices, also had an impact on the flow along $\phi = 180°$.

Concluding Remarks

An experimental study was conducted on a 3-D SW/BLI. The flow field included a steady shock system and 3-D separation with significant cross flow. Surface oil-flow visualization was successful in revealing many details of the surface flow topology. The laser-light-sheet study complemented the surface-topology study even though it did not

yield detailed information of the flow field away from the surface. The postulated flow field included two vortices that left the surface near $\phi = 180°$ and remained embedded in the boundary layer. The pressure documentation was extensive and yielded a contour map of the entire 3-D interaction.

The application of the laser interferometric skin friction technique to the flow was significant in many respects. The technique was used to acquire skin-friction data in a complex, compressible flow that included highly-swept and separated regions. The LISF instrument yielded a mean skin-friction coefficient of $C_{f_x} = 0.00149$ in the upstream, undisturbed boundary layer. The close agreement with two other standards provided assurance of the accuracy of the LISF measurements. The largest source of the uncertainty in the LISF results was the measurement of the model surface temperature. The skin-friction measurements along $\phi = 0°$ downstream of attachment demonstrated an increase of 125% over the upstream value. The amount of increase was higher than along the other two azimuths. Documentation of the 3-D flow along $\phi = 90°$ included LISF measurements in the streamwise direction. Values for the skin friction in the transverse direction were resolved from streamwise LISF measurements and flow-angle data. The resolved data was in close agreement with a limited number of LISF measurements in the transverse direction. Within the separated region along $\phi = 180°$, where the flow was opposite to the free-stream direction, the maximum absolute value of the skin friction reached a value that was 29% of the undisturbed skin-friction level.

Frequently, only pressure measurements are available from SW/BLI experiments to validate computations. Skin-friction measurements, however, offer a more challenging test for computations since skin friction is a better indication of how the viscous stresses are modeled. Thus, the present skin-friction measurements are extremely valuable and significantly enhance the value of this study as a building block experiment for 3-D turbulence modeling and CFD validation.

References

[1]Tanner, L. H., and Blows, L. G., "A Study of the Motion of Oil Films on Surfaces in Air Flow, with Application to the Measurement of Skin Friction", *J. Phys. E: Sci. Instrum.*, Vol. 9, No. 3, 1976, pp. 194-202.

[2]Monson, D. J., Driver, D. M., and Szodruch, J., "Application of a Laser Interferometer Skin-Friction Meter in Complex Flows", *Proc. of the Int'l. Congress on Instrum. in Aero. Simulation Facilities*, 1981, pp. 232-243.

[3]Westphal, R. V., Bachalo, W. D., and Houser, M.H., "Improved Skin Friction Interferometer", NASA TM-88216, 1986.

[4]Kim, K. -S., "Skin Friction Measurements by Laser Interferometry in Supersonic Flows", *Ph.D. Thesis*, Pennsylvania State University, 1989.

[5]Seto, J., and Hornung, H., "Two-Directional Skin Friction Measurement Utilizing a Compact Internally-Mounted Thin-Liquid-Film Skin Friction Meter", AIAA Paper 93-0180, 1993.

[6]Wideman, J. K., "Skin-Friction Measurements in a 3-D, Supersonic Shock-Wave/Boundary-Layer Interaction", *Ph.D. Thesis*, University of Missouri-Columbia, 1993.

[7]Monson, D. J., Mateer, G. G., and Menter, F. R., "Boundary-Layer Transition and Global Skin Friction Measurement with an Oil-Fringe Imaging Technique", SAE Paper 932550, Aerotech '93, 1993.

[8]Bouslog, S., private communication, June, 1991.

[9]Peake, D. J., and Tobak, M., "Three-Dimensional Interactions and Vortical Flows with Emphasis on High Speeds", NASA TM-81169, 1980.

[10]Chapman, G. T., "Topological Classification of Flow Separation on Three-Dimensional Bodies", AIAA Paper 86-0485, 1986.

[11]Batcho, P., and Sullivan J., "The 3-D Flowfield in a Supersonic Shock Boundary Layer Corner Interaction", AIAA Paper 88-0307, 1988.

[12]Cambier, L., and Escande, B., "Calculation of a Three-Dimensional Shock Wave-Turbulent Boundary-Layer Interaction", *AIAA Journal*, Vol. 28, No. 11, 1990, pp. 1901-1908.

[13]Sun, C. -C., and Childs, M. E., "Flowfield Analysis for Successive Oblique Shock Wave-Turbulent Boundary Layer Interactions", NASA CR-2656, 1976.

[14]Hopkins, E.J., "Charts for Predicting Turbulent Skin Friction from the Van Driest Method (II)", NASA TN-D-6945, 1972.